Response of a silicon telescope microdosimeter to 400 AMeV carbon ions

S. Agosteo [a, b, *], M.V. Introini [a, b], A. Pola [a, b], E. Sagia [a]

[a] Politecnico di Milano, Dipartimento di Energia, Sezione di Ingegneria Nucleare, via Ponzio 34/3, 20133 Milano, Italy
[b] Istituto Nazionale di Fisica Nucleare, Sezione di Milano, via Celoria 16, 20133 Milano, Italy

Available online 2 June 2014

1. Introduction

Experimental microdosimetry aims at measuring the fluctuations of energy deposited in individual cells and sub-cellular structures and the microscopic tracks of charged particles (ICRP, 2007). The acquired microdosimetric spectra show the contribution to the absorbed dose of single-event energy depositions in (simulated) microscopic sites. This information is of primary importance for assessing the beam quality of hadrontherapy fields, where the structure of the microscopic track of charged particles plays a fundamental role in cell damage.

The tissue-equivalent proportional counter (TEPCs), the reference detector for microdosimetry, was conceived in 1955 by Rossi and Rosenzweig (1955). It is a proportional counter consisting of a spherical cavity containing a tissue-equivalent (TE) gas. The cavity walls are made of a TE conductive plastic. Microdosimetric sites of tissue are simulated by scaling the pressure of the TE filling gas. This detector and other TEPC-based instruments are still being applied in radiation dosimetry, radiation protection, radiation biology, radiation therapy and radiation chemistry.

Since the last two decades, silicon detectors are being studied (Bradley et al., 2001) as microdosimeters, because they can offer sensitive zones of micrometric dimensions. The silicon detector described in the present work is based on a monolithic silicon telescope.

The first configuration which was studied consists of a single ΔE surface detector 2 μm in thickness (1×1 mm^2 in sensitive area) coupled to an E detector about 500 μm in thickness made out of a single silicon wafer (Fig. 1). The ΔE stage acts as a microdosimeter, while the residual energy E stage allows energy dependent corrections for tissue-equivalence to be performed event-by-event.

This research project has been supported by a Marie Curie Early Initial Training Network Fellowship of the European Community's Seventh Framework Programme under contract number (PITN-GA-2011-289198-ARDENT).

* Corresponding author. Politecnico di Milano, Dipartimento di Energia, Sezione di Ingegneria Nucleare, via Ponzio 34/3, 20133 Milano, Italy. Tel.: +39 02 23996318; fax: +39 02 23996309.
E-mail address: stefano.agosteo@polimi.it (S. Agosteo).

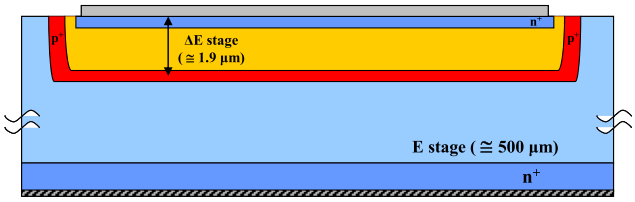

Fig. 1. A schematic view of the first configuration of the monolithic silicon telescope. The detector consists of a ΔE stage (about 1.9 μm of thickness) implanted on a single E stage (500 μm thick).

This feature is fundamental since it enables the comparison of the microdosimetric spectra acquired with the silicon device to the ones acquired with a tissue-equivalent proportional counter (Agosteo et al., 2005, 2006).

The pixelated version of the detector consists of a matrix of micrometric cylindrical diodes (ΔE elements, about 2 μm in thickness and 9 μm in diameter) coupled to a single residual energy stage (E stage), 500 μm in thickness. Thousands of ΔE elements are electrically connected in parallel, giving rise to a single ΔE surface stage of the desired active area (about 0.5 mm^2). Each ΔE element acts as a solid-state microdosimeter, while the residual energy of the impinging particle is measured by the E stage (Agosteo et al., 2008).

A preliminary characterization of the two different detectors was performed by irradiating the devices at different phantom depths with 62 AMeV carbon ions at the test facility of the superconducting cyclotron of the Laboratori Nazionali del Sud – National Institute of Nuclear Physics (INFN-LNS) (Agosteo et al., 2010, in press). Irradiations with 400 AMeV carbon ions are foreseen at the Centro Nazionale di Adroterapia Oncologica (CNAO, National Centre for Oncological Hadrontherapy, Pavia, Italy). For this purpose, the response of a silicon microdosimeter against 400 AMeV carbon ions was calculated with Monte Carlo simulations by using the FLUKA code (Ferrari et al., 2005; Battistoni et al., 2007).

2. Simulation features

The geometry used in the simulations reproduces the one that will be used in the irradiations at CNAO. A parallelepiped PMMA ($C_5H_8O_2$, density 1.19 g cm^{-3}) phantom was irradiated with an expanded, aligned and unmodulated beam of 400 AMeV carbon ion beam (Fig. 2). The simulated beam cross section was 10 × 10 mm^2, the same of the FWHM-transverse size of the one delivered in the CNAO treatment rooms. It should be stressed that active beam delivery system is used at CNAO for distributing the dose to the patient. The detector (10 × 10 mm^2 in active surface) was centered on the beam axis.

For saving computational time, the phantom was divided in two regions: 1) a "high precision" region upstream of the detector, inside the detector and 2) the region downstream of the detector.

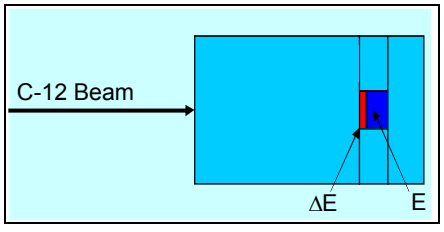

Fig. 2. A schematic view of the simulated geometry that reproduces the one that will be used in the irradiations at the CNAO facility, Pavia, Italy.

The details about the input options for particle transport setting are discussed in the following.

The step length for multiple Coulomb scattering of charged hadrons was set in order to give the 1% of the maximum energy loss in each step (FLUKAFIX input option in the FLUKA code) for all materials considered in the simulations. For electrons the step of multiple Coulomb (EMFFIX input option in the FLUKA code) scattering was set at 5%. A higher value was set in the phantom region downstream of the detector, in order to save computing time.

The cut-off energy for deltaray production (DELTARAY input option in the FLUKA code) was set at 100 keV in all the simulated materials other than the region downstream of the detector which was assigned 1 MeV, again to save computing time. The energy transferred below this cut-off is treated under the continuous energy-loss assumption, while deltaray electrons are transported above. Particle transport was not switched off in the downstream region for simulating, although in an approximate way, their contribution to electron equilibrium in the detector.

Restricted energy-loss fluctuations (i.e. energy straggling) were switched on for charged hadrons and electrons in all the simulated materials (IONFLUCT input option in the FLUKA code). The accuracy of energy-loss fluctuations was set to the minimum allowed value in FLUKA in the region downstream of the detector for saving the computing time.

The energy cut-off for particle transport was set to 1 keV for carbon ions, electron and photons in all regions except for that downstream of the detector (electron and photon cut-off 5 MeV).

The first set of simulations aimed at calculating the depth-dose distribution of primary carbon ions and secondary particles (generated mainly from carbon fragmentation) at various depths across the phantom. Subsequently, microdosimetric spectra were scored in the telescope detector by considering single events of energy deposition inside the ΔE and the residual energy stage. The monolithic detector was placed at various phantom depths. Scatter plots of energy deposited in the ΔE stage against that deposited in the E stage were simulated, thus allowing to discriminate the contribution of carbon ion fragments to the calculated microdosimetric spectra.

3. Results and discussion

As already mentioned, the simulations were performed in order to study the response of the single ΔE-element telescope to 400 AMeV carbon ions, in view of future irradiations at CNAO (Pavia, Italy). The detector was placed at different depths inside the PMMA parallelepiped phantom. The energy deposited in the ΔE and in the E stages was scored event-by-event in order to preserve the correlation between the response of the two elements.

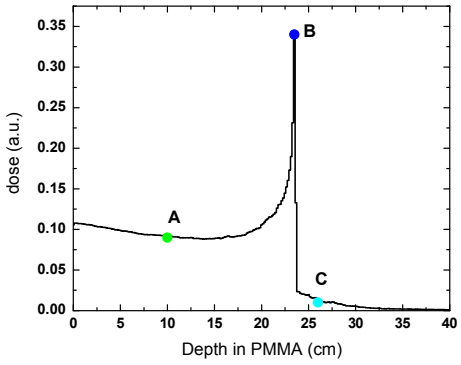

Fig. 3. Depth dose profile of the 400 AMeV unmodulated carbon ion beam. The points A–C are the simulated depths (10, 23.5 and 26 cm, respectively).

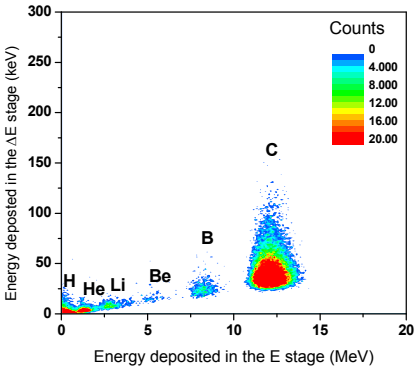

Fig. 4. ΔE–E scatter plot at a shallow phantom depth (position A, Fig. 3, depth 10 cm). Different energy depositions in the two stages allow to distinguish the contribution of the primary beam (C) and of the fragments (B, Be, Li, He, H).

The simulated depths across the Bragg peak were 1 cm, 10 (proximal to the Bragg peak), 23.5 (Bragg peak) and 26 cm (tail of Bragg peak) as shown in Fig. 3. It should be stressed that the depth-dose across the PMMA phantom (Bragg peak, Fig. 3) was scored in regions 1×1 cm^2 wide. This allowed to obtain a sufficient statistics for fragment energy deposition in the tail at depths below the distal part of the Bragg peak. The simulations for calculating the detector response refer to energy deposition in regions 1×1 mm^2 wide, thus decreasing the scoring efficiency of a factor of about 100.

The scatter plot of the energy imparted per event in the ΔE stage versus that deposited in the E stage, at some simulated positions across the Bragg peak are shown in Figs. 4–6.

At the shallowest depth the scatter plot referring to carbon ions resulted to be concentrated in a limited deposition energy interval, since the primary carbon ions are not characterized by a wide energy spread at this depth. The energy spectrum was scored at this depth, showing a quasi-monoenergetic shape. An analogous shape in the scatter plot was observed at 1 cm in depth. The events of energy deposition of ions lighter than carbon are clearly observable in Fig. 4.

The scatter plot simulated in proximity of the Bragg peak (Fig. 5) shows a more structured trend. The upper part of the scatter-plot refers to primary carbon ions depositing their whole energy in both the detector stages. The lower part of the scatter plot refers to higher energy carbon ion which deposit only part of their energy in the whole detector.

The tail below the distal part of the Bragg peak is due to energy deposition from carbon ion fragmentation. The scatter plot

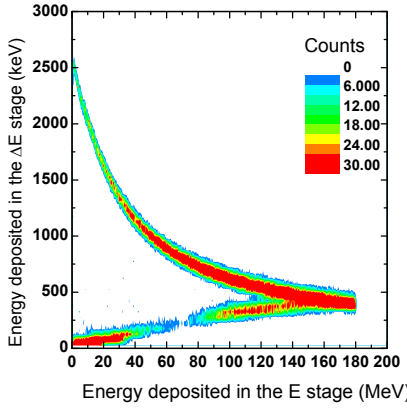

Fig. 5. ΔE–E scatter plot at the Bragg peak (position B, Fig. 3, depth of 23.5 cm). The upper and lower part refer to C ions depositing their whole energy and high energy C ions depositing part of their energy in the detector, respectively.

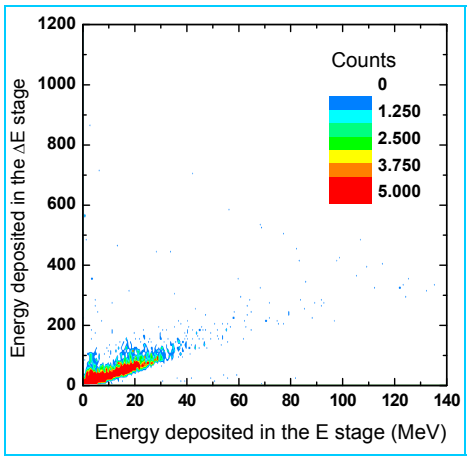

Fig. 6. ΔE–E scatter plot in the tail downstream of the Bragg peak (position C, Fig. 3, depth 26 cm). The events refer to protons from fragmentation and from neutron elastic scattering.

simulated across this tail (Fig. 6) shows events mainly due to protons from fragmentation and elastic scattering from secondary neutrons. Heavier ions cannot be observed because of the insufficient statistics of the simulated data.

The residual energy spectrum acquired in the E stage is shown in Fig. 7. The contribution to the energy spectrum of the primary beam (C) and of its fragments (B, Be, Li, He, H) can be assessed by exploiting the information from the two stages of the detector (scatter plot in Fig. 4),

The microdosimetric distributions were derived by correcting (Agosteo et al., 2010) for tissue-equivalence. The microdosimetric spectra are shown in Figs. 8–11 for the simulated phantom depths.

At the depths proximal to the Bragg peaks (Figs. 8 and 9), the microdosimetric spectra are distributed at low lineal energies, since the slowing-down carbon ions are still of high-energy (hundreds of MeV per nucleon) and therefore of low LET.

Inside Bragg peak, carbon ions slowed-down almost completely and thus show a microdosimetric spectrum (Fig. 10) distributed at higher lineal energies. The edge above 1000 keV μm^{-1} refers to the maximum LET carbon ions.

In the carbon fragment tail (Fig. 11) the simulated events are distributed at low lineal energies below 100 keV μm^{-1}. It should be stressed that these events refer mainly to protons from fragmentation, since heavier ions cannot observed because of the insufficient statistics.

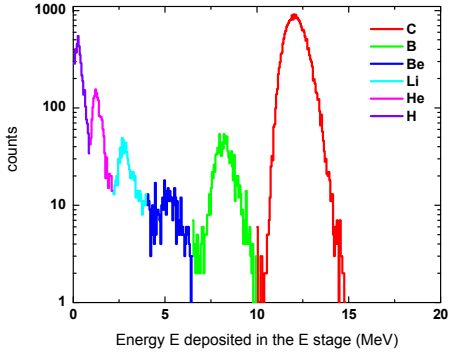

Fig. 7. Residual energy spectrum acquired by the E stage of the detector at the depth of 10 cm (position A, Fig. 3). By exploiting the information of the two stages of the detector (scatter plot in Fig. 4) it is possible to highlight the contribution to the energy spectrum of the primary beam (C) and of the fragments (B, Be, Li, He, H).

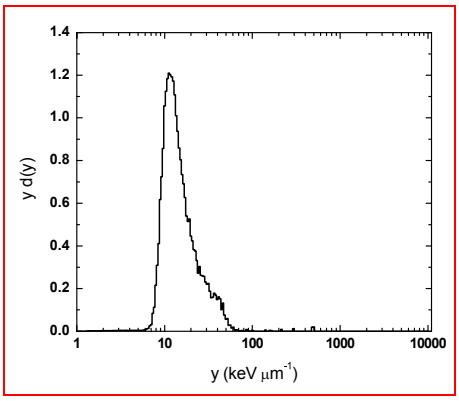

Fig. 8. Microdosimetric spectrum at a depth of 1 cm depth inside the phantom (proximal to the Bragg peak).

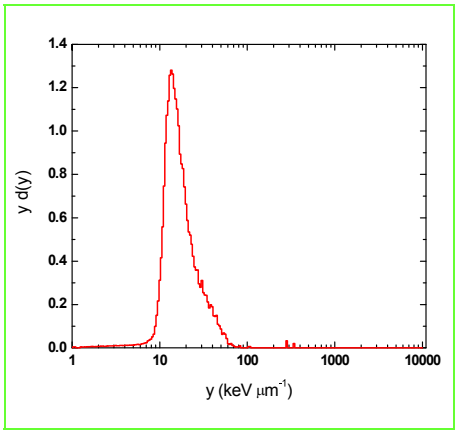

Fig. 9. Microdosimetric spectrum at a depth of 10 cm inside the phantom (proximal to the Bragg peak).

4. Conclusions

Preliminary simulations with the FLUKA Monte Carlo Code were performed in order to study the response to 400 AMeV carbon ions of a monolithic silicon telescope, already proposed for microdosimetry of proton beams. A parallelepiped PMMA phantom was irradiated with an expanded, aligned beam and unmodulated beam of 400 MeV per nucleon carbon ions. The first set of simulations aimed at calculating the energy distribution of ions from carbon fragmentation at various depths across the phantom. Microdosimetric spectra were derived, correcting for tissue-equivalence, by considering single events of energy deposition inside the ΔE elements and the residual energy stage. Scatter plots of energy deposited in the ΔE stage against that deposited in the E stage were exploited to study the contribution of carbon ion fragments to the calculated microdosimetric spectra.

Preliminary results show the potential advantages of using a solid state microdosimeter based on the monolithic silicon telescope technology (effective micrometric-size sites, correction for tissue equivalence event-by-event, fragment discrimination). Similar simulations will be performed for the pixelated silicon telescope and experimental measurements with both detectors will take place at the CNAO facility in 2014, in order to validate the numerical analysis and to verify the capability of measuring microdosimetric spectra of carbon ions by exploiting the proposed

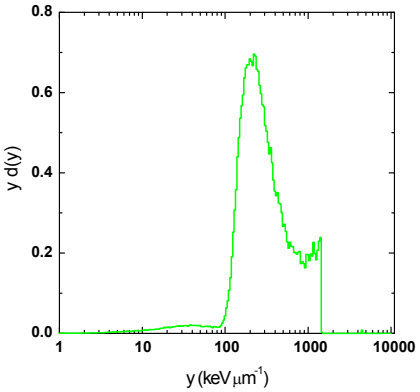

Fig. 10. Microdosimetric spectrum at a depth of 23.5 cm inside the phantom (in the proximity of the Bragg peak).

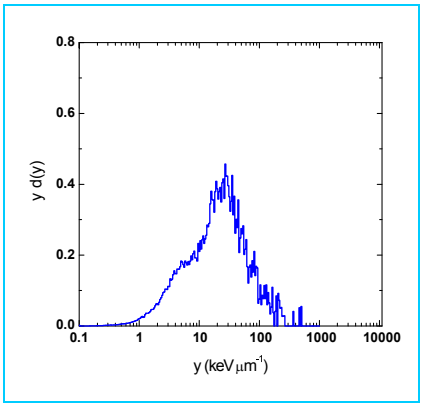

Fig. 11. Microdosimetric spectrum at a depth of 23.5 cm inside the phantom (tail distal to the Bragg peak).

microdosimeter. Measurements are also foreseen with reference TEPCs.

The simulated microdosimetric distributions demonstrated the feasibility of employing the single ΔE stage telescope for measurements in a 400 AMeV carbon beam, since most of the events across the Bragg peak are above the lineal energy threshold (about 10 keV μm^{-1}) imposed by the electronic noise. The microdosimetric spectrum in the fragmentation tail will be partially overwhelmed by the electronic noise, at least for part of the events relating to secondary protons.

References

Agosteo, S., Fallica, P.G., Fazzi, A., Pola, A., Valvo, G., Zotto, P., 2005. A feasibility study of a solid-state microdosimeter. Appl. Radiat. Isot. 63, 529–535.

Agosteo, S., Colautti, P., Fazzi, A., Moro, D., Pola, A., 2006. A solid state microdosimeter based on a monolithic silicon telescope. Radiat. Prot. Dosimetry. 122, 382–386.

Agosteo, S., Fallica, P.G., Fazzi, A., Introini, M.V., Pola, A., Valvo, G., 2008. A pixelated silicon telescope for solid state microdosimetry. Radiat. Meas. 43, 585–589.

Agosteo, S., Cirrone, G.A.P., Colautti, P., Cuttone, G., D Angelo, G., Fazzi, A., Introini, M.V., Moro, D., Pola, A., Varoli, V., 2010. Study of a silicon telescope for the solid state microdosimetry: preliminary measurements at the therapeutic proton beam line of CATANA. Radiat. Meas. 45, 1284–1289.

Agosteo, S., D'Angelo, G., Fazzi, A., Introini, M.V., Pola, A., 2014. A monolithic silicon telescope for hadron beams: numerical and experimental study of the effect of ΔE detector geometry on microdosimetric distributions. Prog. Nucl. Sci. Technol (in press).

Battistoni, G., Muraro, S., Sala, P.R., Cerutti, F., Ferrari, A., Roesler, S., Fassò, A., Ranft, J., 2007. The FLUKA code: description and benchmarking. In: Albrow, M.,

Raja, R. (Eds.), Proceedings of the Hadronic Shower Simulation Workshop, Fermilab 6–8 September 2006, AIP Conference Proceeding, 896, pp. 31–49.
Bradley, P.D., Rosenfeld, A.B., Zaider, M., 2001. Solid state microdosimetry. Nucl. Instrum. Methods B 184, 135–157.
Ferrari, A., Sala, P.R., Fassò, A., Ranft, J., 2005. FLUKA: a Multi-particle Transport Code. CERN-2005-10, INFN/TC_05/11, SLAC-R-773.
International Commission on Radiological Protection, 2007. The 2007 Recommendations of the International Commission on Radiological Protection. ICRP Publication n. 103. Elsevier.
Rossi, H.H., Rosenzweig, W., 1955. A device for the measurement of dose as a function of specific ionization. Radiology 64, 404–411.